Mechanism of dilute-spin-exchange in solid-state NMR

George J. Lu and Stanley J. Opella[a)]
Department of Chemistry and Biochemistry, University of California, San Diego, La Jolla, California 92093-0307, USA

(Received 2 January 2014; accepted 12 March 2014; published online 27 March 2014)

In the stationary, aligned samples used in oriented sample (OS) solid-state NMR, ^{1}H-^{1}H homonuclear dipolar couplings are not attenuated as they are in magic angle spinning solid-state NMR; consequently, they are available for participation in dipolar coupling-based spin-exchange processes. Here we describe analytically the pathways of ^{15}N-^{15}N spin-exchange mediated by ^{1}H-^{1}H homonuclear dipolar couplings. The mixed-order proton-relay mechanism can be differentiated from the third spin assisted recoupling mechanism by setting the ^{1}H to an off-resonance frequency so that it is at the "magic angle" during the spin-exchange interval in the experiment, since the "magic angle" irradiation nearly quenches the former but only slightly attenuates the latter. Experimental spectra from a single crystal of *N*-acetyl leucine confirm that this proton-relay mechanism plays the dominant role in ^{15}N-^{15}N dilute-spin-exchange in OS solid-state NMR in crystalline samples. Remarkably, the "forbidden" spin-exchange condition under "magic angle" irradiation results in ^{15}N-^{15}N cross-peaks intensities that are comparable to those observed with on-resonance irradiation in applications to proteins. The mechanism of the proton relay in dilute-spin-exchange is crucial for the design of polarization transfer experiments. © *2014 AIP Publishing LLC*. [http://dx.doi.org/10.1063/1.4869345]

I. INTRODUCTION

Experiments that result in the exchange of magnetization between two nuclei rank among the most valuable tools in solid-state NMR.[1–3] They characterize molecular structure and dynamics and have a particularly valuable role in the assignment of signals to specific sites in organic and biological molecules.[4] Notably, the through-space coupling of two nuclear spins was the first spin-interaction to be elucidated in the earliest NMR experiments.[5] When two nuclei with spin S = 1/2 are in close spatial proximity, and isolated from other nuclei, then a doublet results in the spectrum due to their dipole-dipole coupling. Importantly, when the coupling is weak because of low-γ or large separation of the (dilute, e.g., ^{13}C or ^{15}N) nuclei, then a doublet may not be observed. However, the weak dipole-dipole couplings that are present are often sufficient for the exchange of magnetization between proximate sites. Multiple coupling pathways including homonuclear spin-diffusion[6,7] have been observed. In essentially all plausible mechanisms, the nuclei in closer proximity yield stronger exchange signals than those with greater separation.

The introduction of the second-order third spin assisted recoupling (TSAR) method of polarization transfer between two low-γ nuclei (^{13}C or ^{15}N) that are both coupled to a third high-γ (^{1}H) nucleus[8] (Figure 1(a)) has led to a renaissance in studies of dilute-spin-exchange spectroscopy.[9–31] Here we demonstrate theoretically and experimentally that the dominant mechanism of spin-exchange between dilute nuclei in a stationary crystalline sample is "mixed-order proton-relay," which relies on transfers between proximate ^{1}H nuclei (Figure 1(b)).

Spin-exchange between ^{15}N nuclei is frequently utilized in protein NMR studies for resonance assignment and structure determination because of the importance of the amide sites located in the polypeptide backbone. TSAR was adapted for stationary, aligned samples in oriented sample (OS) solid-state NMR as the mismatched Hartmann-Hahn (MMHH) condition.[25] TSAR and several other second-order recoupling experiments,[32–34] including proton driven spin diffusion (PDSD),[35,36] rely on the presence of nearby ^{1}H nuclei to transfer magnetization between ^{15}N sites. The ^{1}H nucleus participation in the magnetization transfer is proposed to be through simultaneous coupling to both ^{15}N nuclei. Here we demonstrate that an alternative mechanism is operative, namely polarization transfer through ^{1}H-^{1}H coupling. Notably, this mechanism does not require that each ^{1}H nucleus be coupled to both ^{15}N nuclei. Moreover, it more closely reflects the distribution of nuclei in polypeptides where ^{15}N nuclei are usually located on different residues; only rarely does a ^{1}H nucleus have sizable dipolar couplings to two or more ^{15}N nuclei. By comparing the effects of on-resonance versus "magic-angle" off-resonance ^{1}H spin-lock irradiation[37] it is possible to separate the two transfer mechanisms for dilute-spin-exchange.

II. MATERIALS AND METHODS

The expression, purification, and sample preparation of intact fd bacteriophage have been described previously.[42] ^{15}N-detected solid-state NMR spectra were obtained on a 700 MHz Bruker Avance spectrometer equipped with a home-built ^{1}H/^{15}N double-resonance probe with a strip-shield to

a)Author to whom correspondence should be addressed. Electronic mail: sopella@ucsd.edu

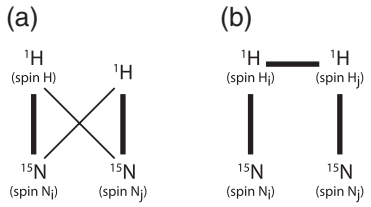

FIG. 1. Schematic drawings of the dipolar coupling networks relevant to ^{15}N-^{15}N dilute-spin-exchange. (a) The second-order TSAR mechanism. (b) The "mixed-order proton-relay" mechanism.

minimize heating of the lossy samples due to the high frequency, high power radiofrequency irradiations.[51]

^{15}N-^{15}N spin exchange experiments on a *N*-acetyl leucine (NAL) single crystal were performed with 45.45 kHz radiofrequency irradiation, 1 ms cross-polarization, 0.1 s Z-filter, and 5 ms mixing time. During mixing, ^{1}H irradiation was elevated to 50 kHz (+10% mismatched condition) for on-resonance spin lock or was dropped to 40.82 kHz with 28.87 kHz offset (+10% mismatched for effective B_1 field). Similarly, the spin exchange experiments on the fd bacteriophage sample used 45.45 kHz irradiation, 1 ms cross-polarization, 0.1 s Z-filter and various mixing times. The control experiment used a 0.1 s Z-filter but no spin-lock spin exchange period. Several mismatched conditions were described above, and notably, the 22% mismatch corresponds to ^{1}H irradiation frequency of 55.6 kHz on resonance or 45.45 kHz with 32 kHz offset. Twenty complex t1 points, 384 complex t2 points, and 400 scans were collected in each experiment. Spectral widths of 10 kHz and 50 kHz were used in the t1 and t2 dimensions, respectively. With a 4 s relaxation delay between each scan, the total time for each experiment was ~ 18 h. For the spectra of 4 s PDSD mixing, the number of scan was reduced to 208, giving approximately the same total experimental time. The spectra for fd bacteriophage were processed with an exponential window function corresponding to 200 Hz line broadening. The data processing and visualization used NMRDraw[52] and Sparky.[53]

Numerical simulations were carried out with SIMPSON 2.0.[54] Numerical simulations of OS solid-state NMR spectra used the same setup as that of the experimental spectra of the NAL single crystal, namely, 45.45 kHz radiofrequency irradiations, 0.1 s Z-filter time, and 5 ms mixing time. Cross-polarization was replaced by putting initial magnetization directly on the two ^{15}N nuclei. The crystal file of "alpha0beta0" was used. The spin networks are shown in the figures. In the simulations of the buildup curves, initial magnetization was put only at one of the ^{15}N nuclei, and the other ^{15}N nucleus was monitored during detection. Only the spin-lock mixing period was simulated with variable length.

III. THEORY OF MIXED-ORDER PROTON-RELAY MECHANISM

Using average Hamiltonian theory, ^{15}N-^{15}N spin exchange can be analyzed in both types of dipolar coupling networks (Figure 1), and we focus the discussion on the terms responsible for the transfer between ^{15}N nuclei in stationary samples. In the case of TSAR, these are the trilinear terms $T_{10}^{H}(T_{1,+1}^{Ni}T_{1,-1}^{Nj} + T_{1,-1}^{Ni}T_{1,+1}^{Nj})$, where spins N_i and N_j are the two ^{15}N and spin H is the ^{1}H.[15] It can be shown that in a simplified scenario of a three-spin system, the change of ^{1}H spin lock irradiation from the on-resonance frequency to the "magic-angle" offset frequency attenuates the amplitude of the polarization transfer according to $\overline{H}_{TSAR}(on\,resonance) \rightarrow \frac{2}{3}\overline{H}_{TSAR}(magic\,angle)$.

In contrast, for the spin network shown in Figure 1(b), three mechanisms can be identified. The first is referred to as the "third-order mechanism." The flip-flop terms between the two ^{15}N nuclei, mediated by a variety of terms derived from the ^{1}H spins, appear in the third-order average Hamiltonian and drive the polarization transfer between the ^{15}N nuclei. The second and third mechanisms are referred to as "multiple-step mechanisms." They involve the first-order and second-order average Hamiltonians and transfer the polarization in more than one step. Collectively they constitute a "mixed-order proton-relay mechanism." It can be shown that most of the terms responsible for ^{15}N polarization transfer are averaged to zero when the ^{1}H spin-lock irradiation is set to the "magic angle;" and the few terms that remain are attenuated by at least an order of magnitude. Thus, a "magic-angle" ^{1}H spin-lock nearly quenches the spin exchange, which can be expressed as $\overline{H}_{proton-relay}(on\,resonance) \rightarrow\sim 0\,(magic\,angle)$. The analytical derivations of these mechanisms are described below.

A. Second-order TSAR mechanism

The second-order TSAR mechanism can be described with a minimum of three spins. Here we consider one ^{1}H spin (spin H) coupled to two ^{15}N spins (spins N_i and N_j) (Figure 1(a)), and for simplicity we omit other internal Hamiltonian terms such as chemical shifts. Using spherical tensor operator notations, the Hamiltonian of the system in the usual rotating frame under a high magnetic field can be written as[38]

$$H(t) = H_{rf}(t) + H_D(t), \tag{1}$$

$$H_D(t) = 2\omega_{H,Ni}T_{10}^{H}T_{10}^{Ni} + 2\omega_{H,Nj}T_{10}^{H}T_{10}^{Nj}. \tag{2}$$

In the absence of magic angle spinning (MAS), the dipolar couplings are not attenuated, and the spatial part of the dipolar coupling Hamiltonian $\omega_{H,Ni}$ and $\omega_{H,Nj}$ are time independent. Note the conversions between spherical tensor operators and the Cartesian spin operators are

$$T_{20}^{AB} = \frac{1}{\sqrt{6}}(3I_{Az}I_{Bz} - \vec{I}_A \cdot \vec{I}_B), \tag{3a}$$

$$T_{2,\pm1}^{AB} = \mp\frac{1}{2}(I_{Az}I_B^{\pm} + I_A^{\pm}I_{Bz}), \tag{3b}$$

$$T_{2,\pm2}^{AB} = \frac{1}{2}I_A^{\pm}I_B^{\pm}, \tag{3c}$$

$$T_{10}^{A} = I_{Az}, \tag{3d}$$

$$T^A_{1,\pm1} = \mp\frac{1}{\sqrt{2}} I^{\pm}_A. \tag{3e}$$

For stationary, aligned samples used in OS solid-state NMR, the pulse sequence of polarization transfer by TSAR usually involves spin-lock pulses on both channels under mismatched Hartmann-Hahn conditions.[25] Therefore, we define the irradiation frequencies of the two channels to be

$$\omega_H = \omega_1 + \Delta\omega, \tag{4a}$$

$$\omega_N = \omega_1, \tag{4b}$$

where $\Delta\omega$ accounts for the mismatched amplitude. The overall effect of the on-resonance spin-lock pulses on ^{15}N can be described as a rotation with the Euler angles

$$R_N\left(\omega_1 t, \frac{\pi}{2}, 0\right) = \exp\{-i\omega_1 t S_z\} \exp\left\{-i\frac{\pi}{2} S_y\right\}. \tag{5a}$$

The spin-lock irradiations on the ^{1}H channel are usually on resonance but here it is generalized to be at any angle θ, for the convenience of subsequent discussions of spin-locking at the "magic angle:"

$$R_H(\omega_1 t, \theta, 0) = \exp\{-i(\omega_1 + \Delta\omega)t I_z\} \exp\{-i\theta I_y\}. \tag{5b}$$

Note the rotation transforms the spin part of the internal Hamiltonian (in this case $H_D(t)$) through the following general transformation equation:

$$R(\alpha, \beta, \gamma) T_{k,q} R^{-1}(\alpha, \beta, \gamma) = \sum_{p=-k}^{+k} T_{k,p} \exp\{-i\alpha p\} d^k_{p,q}(\beta) \exp\{-i\gamma q\}. \tag{6}$$

This provides a convenient way of analyzing pulse sequences, such as deriving the following interaction frame Hamiltonian:

$$\tilde{H}_{\text{int}} = U^{-1}_{rf}(t_0, t_0 + \tau) H_{\text{int}} U_{rf}(t_0, t_0 + \tau). \tag{7}$$

In the current case, H_{int} includes only the H_D described in Eq. (2). The relative ease of performing spin rotation calculations is the main reason for using spherical tensors instead of Cartesian tensors.

The time propagator can then be approximated using Average Hamiltonian Theory with stroboscopic observation from time t_0 to $t_0 + \tau$,

$$U(t_0 + \tau) \cong U_{rf}(t_0, t_0 + \tau) \exp\{-i\overline{H}\tau\}, \tag{8}$$

where $\overline{H}$ is the average Hamiltonian. Using a Magnus expansion, the first few terms in $\overline{H}$ are represented using the general formulae of Bialynicki–Birula *et al.*:[39]

$$\overline{H}^{(1)} = \frac{1}{\tau}\int_{t_0}^{t_0+\tau} \tilde{H}_{\text{int}} dt, \tag{9a}$$

$$\overline{H}^{(2)} = -\frac{i}{2\tau}\int_{t_0}^{t_0+\tau} dt_1 \int_{t_0}^{t_0+t_1} dt_2 [\tilde{H}_{\text{int}}(t_1), \tilde{H}_{\text{int}}(t_2)], \tag{9b}$$

$$\overline{H}^{(3)} = -\frac{1}{6\tau}\int_{t_0}^{t_0+\tau} dt_1 \int_{t_0}^{t_0+t_1} dt_2 \int_{t_0}^{t_0+t_2} dt_3 ([\tilde{H}_{\text{int}}(t_1), [\tilde{H}_{\text{int}}(t_2), \tilde{H}_{\text{int}}(t_3)] + [\tilde{H}_{\text{int}}(t_3), [\tilde{H}_{\text{int}}(t_2), \tilde{H}_{\text{int}}(t_1)]]). \tag{9c}$$

Notably, the order numbers in the second-order TSAR mechanism and mixed-order proton-relay mechanisms refer to the number described here during the Magnus expansion. Since spin lock irradiations in this class of experiments usually last for several milliseconds, we can assume that both $\omega_1\tau$ and $\Delta\omega\tau$ satisfy the integers of 2π. Explicitly, this can be written as

$$\tau = \frac{2\varepsilon_1\pi}{\omega_1} = \frac{2\varepsilon_2\pi}{\Delta\omega}, \tag{10}$$

where ε_1 and ε_2 are both integers.

For the minimal three-spin system and the simplified internal Hamiltonian, we can explicitly evaluate the first two orders in the Magnus expansion using Mathematica with the assistance of scripts from MathNMR[40] and SpinDynamica:[41]

$$\overline{H}^{(1)} = 0, \tag{11a}$$

$$\overline{H}^{(2)}_I = -\frac{2\omega_{H,Ni}\omega_{H,Nj}(\omega_1 + \Delta\omega)sin^2(\theta)}{\Delta\omega(2\omega_1 + \Delta\omega)} \times T^H_{10}\left(T^{Ni}_{1,+1}T^{Nj}_{1,-1} + T^{Ni}_{1,-1}T^{Nj}_{1,+1}\right), \tag{11b}$$

$$\overline{H}^{(2)}_{II} = \frac{1}{2\omega_1\Delta\omega(2\omega_1 + \Delta\omega)} \times (\omega_1(\omega_1 + \Delta\omega)\left(\omega^2_{H,Ni} + \omega^2_{H,Nj}\right)sin^2(\theta)T^H_{10} + (\Delta\omega(2\omega_1 + \Delta\omega)cos^2(\theta) - \omega^2_1 sin^2(\theta)) \times (\omega^2_{H,Ni}T^{Ni}_{10} + \omega^2_{H,Nj}T^{Nj}_{10})). \tag{11c}$$

The most relevant Hamiltonian is $\overline{H}^{(2)}_I$ in Eq. (11b), which contains the three-spin trilinear terms for polarization transfer between spins N_i and N_j; the magnitude of this term has a $sin^2(\theta)$ relationship with the ^{1}H channel spin-lock angle θ. Therefore, the term is only attenuated when the ^{1}H spin-lock pulse is changed from the on-resonance condition ($\theta = \pi/2$) to the "magic-angle" condition:

$$\overline{H}^{(2)}_I(on\ resonance) \rightarrow \frac{2}{3}\overline{H}^{(2)}_I(magic\ angle). \tag{12}$$

B. Third-order mechanism

For the proton-relay mechanism diagrammed in Figure 1(b), the minimal system contains four spins, rather than the three spins of the TSAR mechanism. It is straightforward to envision that the key flip-flop terms between the two ^{15}N atoms would appear in the third-order average Hamiltonian terms. We can use the same set of formulae described in the last section to derive this mechanism. We denote the two ^{1}H spins to be H_i and H_j and the two ^{15}N spins to be N_i and N_j (Figure 1(b)), and the internal Hamiltonian now contains:

$$H_D(t) = \sqrt{6}\omega_{Hi,Hj}T^{Hi,Hj}_{20} + 2\omega_{Hi,Ni}T^{Hi}_{10}T^{Ni}_{10} + 2\omega_{Hj,Nj}T^{Hj}_{10}T^{Nj}_{10}. \tag{13}$$

The third order average Hamiltonian evaluated from Eq. (9c) contains many terms; for simplicity, we only

evaluate those terms containing zero-quantum flip-flop terms between spin N_i and N_j $T^{Ni}_{1,+1}T^{Nj}_{1,-1} + T^{Ni}_{1,-1}T^{Nj}_{1,+1}$. It is noted that double-quantum terms also exist in addition to the zero-quantum terms that we quantify here, as those analyzed for TSAR mechanism.[9,15] The zero-quantum terms include:

$$\overline{H}^{(3)}_{I} = T^{Hi}_{10}T^{Hj}_{10}\left(T^{Ni}_{1,+1}T^{Nj}_{1,-1} + T^{Ni}_{1,-1}T^{Nj}_{1,+1}\right)\omega_{Hi,Hj}\omega_{Hi,Ni}\omega_{Hj,Nj}sin^2(\theta) \times \frac{4\omega_1^2 - 2\omega_1\Delta\omega - \Delta\omega^2 + 3(4\omega_1^2 - 6\omega_1\Delta\omega - 3\Delta\omega^2)cos(2\theta)}{2\Delta\omega^2(2\omega_1 + \Delta\omega)^2}, \tag{14a}$$

$$\overline{H}^{(3)}_{II} = \left(T^{Hi}_{1,+1}T^{Hj}_{1-1} + T^{Hi}_{1,-1}T^{Hj}_{1,+1}\right)\left(T^{Ni}_{1,+1}T^{Nj}_{1,-1} + T^{Ni}_{1,-1}T^{Nj}_{1,+1}\right)\omega_{Hi,Hj}\omega_{Hi,Ni}\omega_{Hj,Nj} \times \left(\frac{-2\omega_1^4 + 4\omega_1^3\Delta\omega - 18\omega_1^2\Delta\omega^2 - 20\omega_1\Delta\omega^3 - 5\Delta\omega^4}{4\omega_1^2\Delta\omega_1^2(2\omega_1 + \Delta\omega)^2} + \frac{\left(8\omega_1^4 + 8\omega_1^3\Delta\omega - 28\omega_1^2\Delta\omega^2 - 32\omega_1\Delta\omega^3 - 8\Delta\omega^4\right)cos(2\theta)}{4\omega_1^2\Delta\omega_1^2(2\omega_1 + \Delta\omega)^2} + \frac{3(-2\omega_1^4 - 4\omega_1^3\Delta\omega - 6\omega_1^2\Delta\omega^2 - 4\omega_1\Delta\omega^3 - \Delta\omega^4)cos(4\theta)}{4\omega_1^2\Delta\omega_1^2(2\omega_1 + \Delta\omega)^2}\right), \tag{14b}$$

$$\overline{H}^{(3)}_{III} = \left(T^{Hi,Hj}_{2,+1} + T^{Hi,Hj}_{2,-1}\right)\left(T^{Ni}_{1,+1}T^{Nj}_{1,-1} + T^{Ni}_{1,-1}T^{Nj}_{1,+1}\right)\omega_{Hi,Hj}\omega_{Hi,Ni}\omega_{Hj,Nj}\frac{-sin(2\theta)(3cos^2(\theta) - 1)}{\sqrt{2}\Delta\omega(2\omega_1 + \Delta\omega)}, \tag{14c}$$

$$\overline{H}^{(3)}_{IV} = \left(T^{Hi,Hj}_{2,+2} + T^{Hi,Hj}_{2,-2}\right)\left(T^{Ni}_{1,+1}T^{Nj}_{1,-1} + T^{Ni}_{1,-1}T^{Nj}_{1,+1}\right)\omega_{Hi,Hj}\omega_{Hi,Ni}\omega_{Hj,Nj}\frac{-2sin^2(\theta)(3cos^2(\theta) - 1)}{\Delta\omega(2\omega_1 + \Delta\omega)}. \tag{14d}$$

We note that $\overline{H}^{(3)}_{I}$ and $\overline{H}^{(3)}_{II}$ contain a mixture of the term $T^{Hi,Hj}_{20}(T^{Ni}_{1,+1}T^{Nj}_{1,-1} + T^{Ni}_{1,-1}T^{Nj}_{1,+1})$ and other terms that originate from commutation between homonuclear and heteronuclear dipolar couplings.

In the next step, we evaluate the dependence of these flip-flop terms in the third-order average Hamiltonian on the ^{1}H channel with spin-lock angle θ. We can readily see both $\overline{H}^{(3)}_{III}$ and $\overline{H}^{(3)}_{IV}$ vanish when θ is the magic angle. $\overline{H}^{(3)}_{I}$ and $\overline{H}^{(3)}_{II}$ do not vanish at the magic angle but are reduced by factors of around 18 and 16, respectively, if one assumes the ratio $\omega_1/\Delta\omega = 10$, i.e., the 10% mismatched condition previously shown to be optimal for ^{15}N-^{15}N spin exchange in a NAL crystal.[25] This is summarized below for a comparison with Eq. (12):

$$\overline{H}^{(3)}_{I}\left(on\,resonance, \frac{\omega_1}{\Delta\omega} = 10\right) \rightarrow\sim \frac{1}{18}\overline{H}^{(3)}_{I}\left(magic\,angle, \frac{\omega_1}{\Delta\omega} = 10\right), \tag{15a}$$

$$\overline{H}^{(3)}_{II}\left(on\,resonance, \frac{\omega_1}{\Delta\omega} = 10\right) \rightarrow\sim \frac{1}{16}\overline{H}^{(3)}_{II}\left(magic\,angle, \frac{\omega_1}{\Delta\omega} = 10\right), \tag{15b}$$

$$\overline{H}^{(3)}_{III}(on\,resonance) \rightarrow 0(magic\,angle), \tag{15c}$$

$$\overline{H}^{(3)}_{IV}(on\,resonance) \rightarrow 0\,(magic\,angle). \tag{15d}$$

Interestingly, $\overline{H}^{(3)}_{I}$ and $\overline{H}^{(3)}_{II}$ reaches zero when the ^{1}H channel spin-lock angle θ is 52.92° and 56.53°, respectively. Both of the angles are very close to the magic angle of 54.7°.

C. Multiple-step mechanisms and repolarization of ^{1}H

Other pathways for polarization transfer from one ^{15}N atom to the other in the same four-spin system (Figure 1(b)) are through multiple-step polarization transfer via ^{1}H. They can also be viewed as proton-relay mechanisms, and their difference from the one described in the last section is that the Hamiltonian terms in the above section can convert polarization in the first ^{15}N (expressed as I^{Ni}_z) directly to the polarization in the second one (I^{Nj}_z), while the mechanisms described here convert polarization I^{Ni}_z to I^{Hi}_z (the first ^{1}H) or I^{Hj}_z (the second ^{1}H) and then, in the subsequent step, to I^{Nj}_z. These pathways are summarized in Figure 2.

We start by deriving the second-order average Hamiltonian terms for the four-spin system. Similar to the case of the TSAR mechanism, trilinear terms involving three spins appear as $T^{Hi}_{10}(T^{Ni}_{1,+1}T^{Hj}_{1,-1} + T^{Ni}_{1,-1}T^{Hj}_{1,+1})$ and $T^{Hj}_{10}(T^{Hi}_{1,+1}T^{Nj}_{1,-1} + T^{Hi}_{1,-1}T^{Nj}_{1,+1})$. The term $T^{Hi}_{10}(T^{Ni}_{1,+1}T^{Hj}_{1,-1} + T^{Ni}_{1,-1}T^{Hj}_{1,+1})$ can transfer polarization from spin N_i (a ^{15}N nucleus) to spin H_j (a ^{1}H nucleus). In contrast to the TSAR mechanism, which

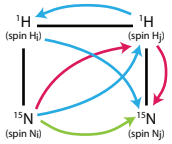

FIG. 2. Schematic drawing of the pathways for spin exchange from one ^{15}N atom to the other. (Green) Third-order proton-relay mechanism. (Magenta) Second-order two-step mechanism. (Cyan) Mixed-order three-step mechanism.

involves only heteronuclear couplings, spins H_i and H_j are coupled through homonuclear dipolar couplings, and therefore additional trilinear terms in the form of $T_{10}^{Hj}(T_{1,+1}^{Hi}T_{1,-1}^{Ni} + T_{1,-1}^{Hi}T_{1,+1}^{Ni})$ and $T_{10}^{Hi}(T_{1,+1}^{Hj}T_{1,-1}^{Nj} + T_{1,-1}^{Hj}T_{1,+1}^{Nj})$ also appear. The term $T_{10}^{Hi}(T_{1,+1}^{Hj}T_{1,-1}^{Nj} + T_{1,-1}^{Hj}T_{1,+1}^{Nj})$ can thus transfer magnetization from spin H_j to spin N_j. The relevant second-order Hamiltonian terms for these two steps are extracted out:

$$\overline{H}_I^{(2)} = T_{10}^{Hi}\left(T_{1,+1}^{Ni}T_{1,-1}^{Hj} + T_{1,-1}^{Ni}T_{1,+1}^{Hj}\right) \times \omega_{Hi,Hj}\omega_{Hi,Ni}sin(\theta)\frac{1-3cos^2(\theta)}{2\Delta\omega}, \quad (16a)$$

$$\overline{H}_{II}^{(2)} = T_{10}^{Hi}\left(T_{1,+1}^{Hj}T_{1,-1}^{Nj} + T_{1,-1}^{Hj}T_{1,+1}^{Nj}\right) \times \omega_{Hi,Hj}\omega_{Hj,Nj}sin(\theta)\frac{1-3cos^2(\theta)}{\Delta\omega}. \quad (16b)$$

Then the evolution of density matrix can be followed through the formulae

$$\rho(t) = \exp(-iHt)\rho(t_0)\exp(iHt). \quad (17)$$

When $\rho(t_0) = I_z^{Ni}$, we can obtain non-zero I_z^{Hj} and I_z^{Nj} in $\rho(t)$.

Similarly, polarization transfer from spin N_i to spin N_j can occur in three steps (cyan color, Figure 2). In the first step, the same second-order Hamiltonian terms (Eq. (16a)) transfers polarization to spin H_j. In the second step, the first-order Hamiltonian term will drive the polarization to spin H_i. The first-order Hamiltonian contains only the homonuclear dipolar coupling,

$$\overline{H}^{(1)} = \sqrt{6}\omega_{Hi,Hj}T_{20}^{Hi,Hj}\frac{3cos^2(\theta)-1}{2}. \quad (18)$$

Lastly, the trilinear term will transfer magnetization from spin H_i to spin N_j:

$$\overline{H}_{III}^{(2)} = T_{10}^{Hj}\left(T_{1,+1}^{Hi}T_{1,-1}^{Nj} + T_{1,-1}^{Hi}T_{1,+1}^{Nj}\right) \times \omega_{Hi,Hj}\omega_{Hj,Nj}sin(\theta)\frac{1-3cos^2(\theta)}{2\Delta\omega}. \quad (19)$$

The important realization is again that all relevant terms in Eqs. (16), (18), and (19) have a $1 - 3cos^2(\theta)$ dependence on the ^{1}H channel spin-lock angle θ. Therefore, these mechanisms of polarization transfer will also be quenched by setting the ^{1}H channel spin-lock irradiation at the magic angle.

Another difference of these two mechanisms from the one shown in the last section is that they lead to repolarization of ^{1}H. Due to their large differences in gyromagnetic ratios, the cross- polarization from low-γ nuclei back to high-γ nuclei usually causes substantial depolarization of the former. Since ^{1}H usually experiences shorter $T_{1\rho}$ and faster decay, their repolarization during spin exchange may become a pathway to drain the magnetization. This is related to one of the speculated reasons for the performance of these pulse sequences in biological sample, which will be discussed in Sec. V.

IV. NUMERICAL SIMULATIONS AND EXPERIMENTAL RESULTS

The analytical results described in Sec. III have shown that by switching the ^{1}H irradiation frequency from on-resonance to off-resonance at the magic angle, the "mixed-order proton-relay" mechanism will be nearly quenched, while the TSAR mechanism will only be slightly attenuated. This suggests an experimental method to differentiate the two mechanisms by comparing the polarization transfer efficiency in the presence of on-resonance and off-resonance "magic-angle" ^{1}H irradiation. The numerical simulations of the two-dimensional ^{15}N-^{15}N spin exchange spectra (Figures 3(a)–3(d)) and the magnetization buildup curve (Figure 4) validate the conclusions. The dipolar coupling networks used for simulation of the different mechanisms are drawn on the left of Figures 3(a)–3(d). The TSAR mechanism (Figures 3(a) and 3(b)) relies on the same ^{1}H being coupled to two ^{15}N atoms, but the proton-relay mechanisms (Figures 3(c) and 3(d)) do not. Instead, proton-relay mechanisms transfer polarization via ^{1}H-^{1}H homonuclear dipolar couplings. In the simulated spectra, all expected cross-peaks are visible, except for those in Figure 3(d), which supports the theoretical result of "magic-angle" irradiation suppressing polarization transfers via proton-relay mechanisms.

The comparison of the two experimental spectra obtained from a single crystal of NAL (Figures 3(e) and 3(f)) shows nearly completely quenched spin exchange in the presence of the "magic-angle" spin-lock irradiation, which demonstrates that the proton-relay mechanism is the main contributor to the ^{15}N-^{15}N spin exchange. The spin-lock contact time is 5 ms for both simulations and experiments, and during this interval the cross-peaks in Figure 2(e) approach saturation, since their intensities are nearly the same as the diagonal peaks. For the spectrum in Figure 2(f), however, we observed continuing but slow buildup beyond 9 ms, the longest duration tested. This agrees with the simulation of the polarization buildup (Figure 4(d)). MMHH contact times around 5 ms are most relevant with the consideration of applying these pulse sequences to protein samples in OS solid-state NMR, because their shorter $T_{1\rho}$ values usually results in loss of signal intensity at longer mixing times.[30,31,37,42]

Under MAS conditions, the proton-relay mechanism is suppressed because of the averaging of homonuclear dipolar couplings. The extent of suppression is directly related to the spinning speed. This might provide a partial explanation for the contrast between the mixing times used in MAS solid-state NMR and OS solid-state NMR. In ^{15}N-^{15}N correlation experiments under MAS condition,[10] the mixing time is typically 20 ms but most of the observed cross-peaks are sequential in helix (~3 Å) or β-sheet (< 5 Å) structures. By contrast,

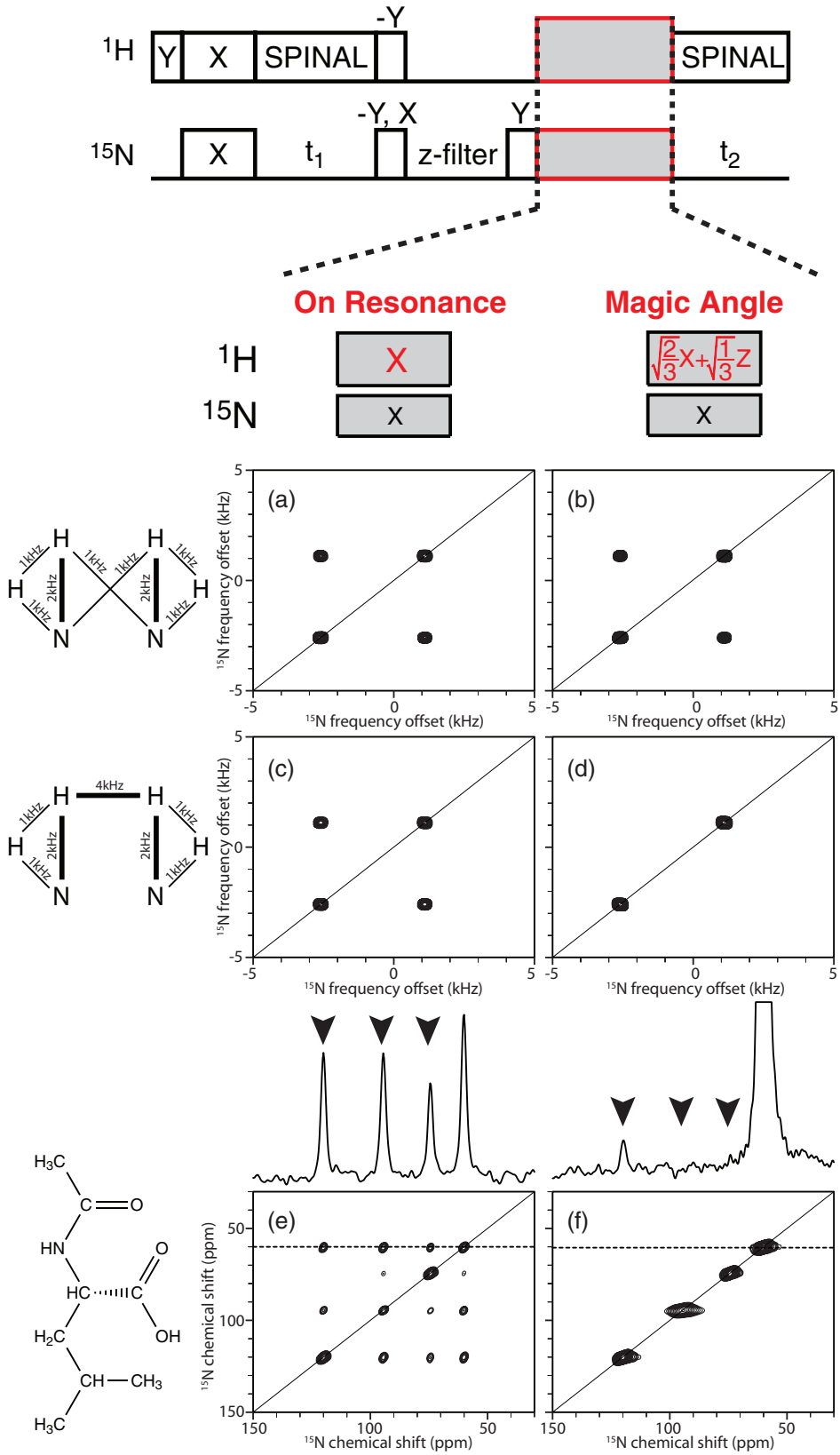

FIG. 3. Numerical simulation and experimental ^{15}N-^{15}N spin exchange spectra that differentiate TSAR and proton-relay mechanisms by ^{1}H spin-lock pulses on-resonance or off-resonance at the magic angle. The pulse sequences are drawn on the top. (a)–(d) are simulated spectra. (e) and (f) are experimental spectra. (a), (c), and (e) are with on-resonance ^{1}H spin-lock irradiation. (b), (d), and (f) are with "magic-angle" ^{1}H spin-lock irradiation. (a) and (b) Numerical simulation on the spin network for the TSAR mechanism, where "magic-angle" irradiation only slightly attenuates the spin exchange. (c) and (d) Numerical simulation on the spin network for proton-relay mechanisms, where "magic-angle" irradiation nearly quenches the spin exchange. (e) and (f) Experimental results obtained from the NAL single crystal sample. The arrows indicate the cross-peaks resulting from spin-exchange. Notably, the four resonances arise from the four uniquely oriented amide sites in each unit cell of an NAL crystal.

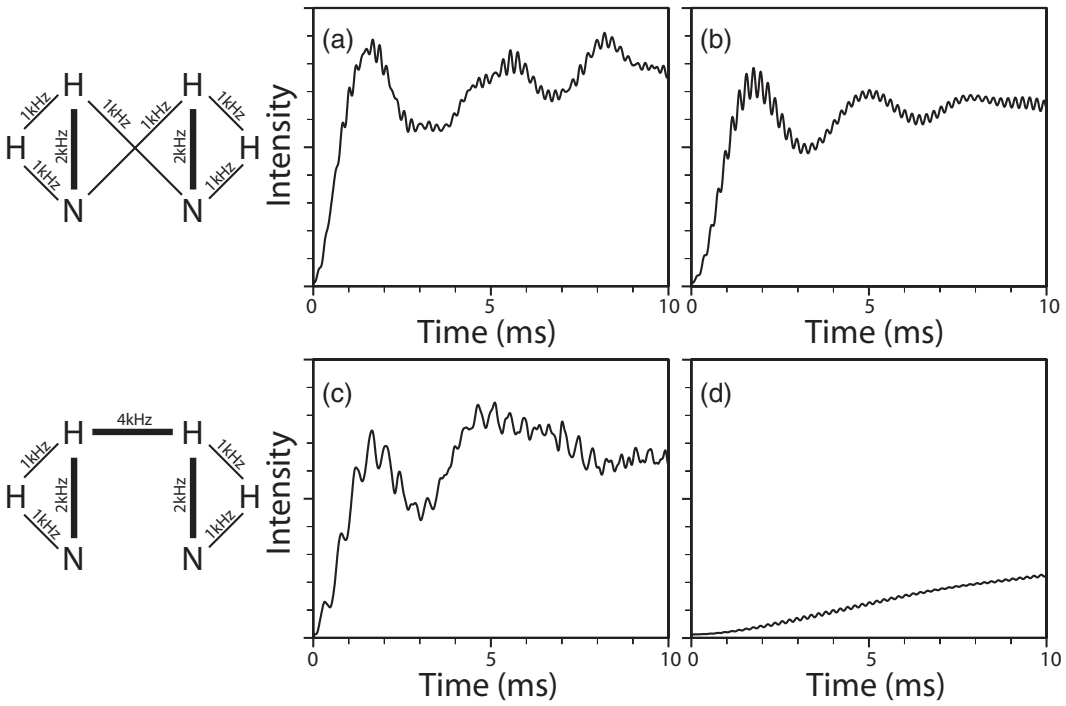

FIG. 4. Numerical simulation of the polarization buildup curve resulting from ^{15}N-^{15}N spin-exchange. (a) and (c) On-resonance ^{1}H spin-lock pulse. (b) and (d) Magic-angle ^{1}H spin-lock pulse. Drawn on the left are the spin networks proposed for TSAR mechanism (top row) and for mixed-order proton-relay mechanism (bottom row).

in OS solid-state NMR, most reports show that 5 ms mixing provides all cross-peaks among ^{15}N spins in a NAL single crystal, which has inter-molecular ^{15}N-^{15}N distances greater than 6.5 Å. Under slow spinning, the incomplete averaging of homonuclear couplings makes the situation resemble that encountered in OS solid-state NMR, but this requires an analysis beyond that in this article.

V. DILUTE SPIN EXCHANGE IN PROTEINS

A. Selectively ^{15}N-Val labeled fd bacteriophage

To optimize the spin exchange conditions and to test the different effects of on-resonance and "magic-angle" ^{1}H spin-lock pulses to protein samples, multiple spectra need to be collected, and in each spectrum, the signals must have reasonably large signal-to-noise ratios. Additionally, for quantification a signal would ideally be from an isolated cross-peak involving only one pair of assigned ^{15}N nuclei rather than a cluster of cross-peaks.

Considering all these criteria, we have chosen to perform experiments on a magnetically aligned sample of selectively ^{15}N-Val labeled fd bacteriophage. The high-resolution structure of the major coat protein in intact fd bacteriophage has been solved by OS solid-state NMR.[42] Interestingly, the sequence of the fd coat protein contains four nearby valines, V29, V30, V31, and V33. The first three valines are sequential and can be tested for sequential resonance assignments, while the spin exchange with V33 can be potentially used for longer-range i/i+3 and i/i+4 spin exchange experiments. The four valine signals are reasonably well separated in one-dimensional OS solid-state NMR spectrum.[42] These properties allow us to perform multiple 18-h experiments to test each spin exchange condition and monitor the cross-peak intensity for a single pair of ^{15}N nuclei with a signal-to-noise ratio greater than 6:1, which can be difficult to obtain with other protein samples.[31]

In the example spectra (Figure 5(a)), cross-peaks from the V29/V30 and V30/V31 pairs are of sizable intensity. Since the cross-peaks of V30/V31 are close to the diagonal, we focus on the two cross-peaks of V29/V30 for the quantification and systematic comparison of intensities. Cross-peaks involving V33 are near or below the noise level in the current experiments. Therefore, the characterization of long-range spin exchange may require longer signal averaging or the development of stronger samples, and is beyond the scope of the present study. The pulse length and mismatch percentage between ^{1}H and ^{15}N channels are the first parameters to optimize (Figure 5(b)), and on-resonance ^{1}H spin-lock pulses are used in this case. While in all spectra a 5 ms pulse length yields the highest intensity, a 22% mismatch has provided slightly higher intensity than other conditions. This optimal mismatch percentage agrees with the previously found optimal condition for the similar filamentous Pf1 bacteriophage.[31] Therefore, we chose 5 ms length and 22% mismatch for the comparison between on-resonance and "magic-angle" ^{1}H spin-lock pulses (Figure 5(c)). Remarkably, the results are quite different from those obtained from the NAL single crystal. While the "magic-angle" ^{1}H spin-lock irradiation nearly quenches the spin exchange in the NAL single crystal, it provides better results than the on-resonance pulse in the aligned sample of fd bacteriophage. It should be noted that the highest cross-peak intensity using "magic-angle" irradiation appears in the spectrum with 7 ms mixing time, rather than 5 ms mixing

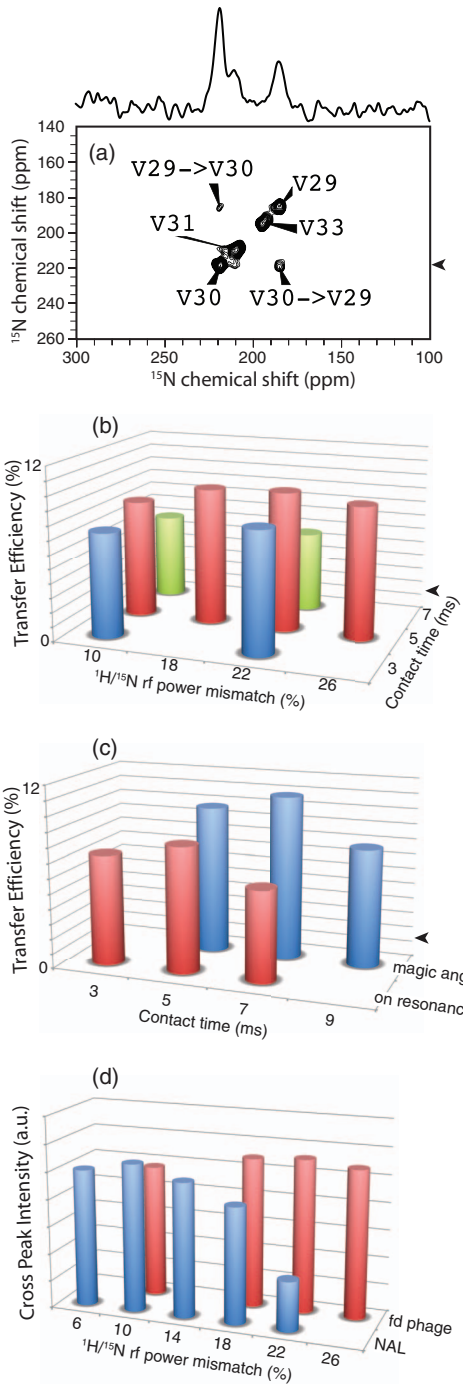

FIG. 5. Experimental optimization of ^{15}N-^{15}N spin exchange condition in the sample of ^{15}N-Val labeled intact fd bacteriophage. (a) An example spectrum and the resonance assignments. The arrow indicates where the one-dimensional slice is extracted. The average intensity of the two well-separated cross-peaks between V29 and V30 are used to quantify the spin exchange efficiency. (b) Optimization of the mismatch percentage and contact time with on-resonance ^{1}H channel spin-lock pulse. (c) Comparison of cross-peak intensity between the on-resonance and magic-angle ^{1}H spin-lock pulses, with the mismatch percentage maintained at 22%. Transfer efficiency is calculated by dividing the cross-peak intensity in the experiments by the main peak intensity in the control experiment, which uses a 0.1 s Z-filter and no spin-lock pulses.[30] Notably, the mismatch percentage for magic-angle pulses is calculated from the ratio of B_{eff} of ^{1}H channel and B_1 of ^{15}N channel; by contrast, the ratio of the two B_1 fields is used in the calculation for on-resonance pulses. (d) The sensitivity to the mismatch percentage is different between NAL single crystal and fd phage sample. Cross-peak intensities are plotted in an arbitrary scale (a.u.).

time in those spectra using on-resonance irradiation, possibly because the "magic-angle" spin-lock lengthens $T_{1\rho}$. We have also tested "magic-angle" ^{1}H spin-lock pulses on a sample of the membrane-bound form of uniformly ^{15}N-labeled Pf1 coat protein in magnetically aligned bicelles. The data showed strong cross-peaks from ^{15}N-^{15}N spin exchange, which are about the same intensity as those from on-resonance irradiations.

In conclusion, the experimental results from protein samples undergoing global motions, such as filamentous bacteriophage particles and membrane proteins rotating about the bilayer normal, are in contrast to the analytical derivations and experimental results from the NAL single crystal. While the "magic-angle" ^{1}H spin-lock irradiation nearly quenches the spin exchange in a single crystal, in proteins it provides strong cross-peaks that are of similar intensities as the on-resonance case. This phenomenon may result from the combined effect of several underlying mechanisms, which are discussed in Sec. V B.

B. Discussion of motion interference and spin exchange distance

We recently generalized the "motion-adapted" properties of a homonuclear decoupling sequence MSHOT-Pi4/Pi, whose performance is especially efficient for membrane protein samples but not for single crystals.[43,44] The underlying mechanism of the "motion-adapted" property was characterized theoretically and experimentally as the interference between the protein's rotational exchange motion and the radiofrequency pulses. Importantly, in recent work to apply multiple contact cross-polarization to enhance signals, Nevzorov and co-workers observed much more pronounced signal enhancement for membrane protein sample than for NAL single crystal,[45,46] and this technique was later adapted to enhance signals in MAS solid-state NMR on membrane proteins undergoing rotational diffusion.[47] Another study analyzed the effect of the static disorder and uniaxial rotational diffusion of the protein samples on the appearance of separated local field spectra and showed evidence of inhomogeneously broadened line widths.[48] Here the discovery that a "magic-angle" ^{1}H spin-lock pulse is a "forbidden" condition in a single crystal but provides better ^{15}N-^{15}N spin exchange in a bacteriophage sample, is to a certain extent, another case of a "motion-adapted" sequence and may have its roots in a similar underlying mechanism.

This speculation is supported theoretically, since we previously showed that a "magic-angle" ^{1}H spin-lock pulse (i.e., Lee-Goldberg condition) has the highest susceptibility to motional interference, compared to other homonuclear decoupling sequences such as SAMPI4 and MSHOT-Pi4.[44] The reason is because in the first-order average Hamiltonian,

$$\overline{H}^{(1)} = \frac{1}{\tau}\int_{t_0}^{t_0+\tau} dt\sqrt{6}\omega_D \times \sum_{m=-2}^{+2} T_{2m}^{AB}\exp\{-im\omega_{eff}t\}d_{m0}^{2}(\theta_{magic}), \quad (20)$$

the spatial component, ω_D, of the homonuclear dipolar coupling, which becomes time-dependent as a result of sample rotational motion, interferes with the averaging of $\exp\{-im\omega_{eff}t\}$ and causes the Hamiltonian term to become non-zero. The same effect occurs for most of the Hamiltonians discussed in this article. Note that all the Hamiltonian terms shown in Eqs. (11), (14), (16), (18), and (19) are calculated by integration over the τ period under the assumption that dipolar couplings $\omega_{Hi,Hj}$, $\omega_{Hi,Ni}$, and $\omega_{Hj,Nj}$ are time-independent. These terms will have more complicated dependence on the ^{1}H spin lock angle θ, and many additional terms would appear if the spatial part of the dipolar couplings interferes with their averaging by the term $\exp\{-im\omega t\}$. Therefore, we could qualitatively conclude that, when motion interference effects exist for a protein undergoing global reorientation, the "magic-angle" ^{1}H spin-lock pulse becomes much less efficient in stopping the polarization transfer through ^{1}H-^{1}H homonuclear dipolar couplings, and this condition is no longer "forbidden."

Similarly, sample motions can also cause the Hartmann-Hahn match or mismatch condition to be more promiscuous in protein samples. For example, rotational motions at the mismatched frequency can partially recreate the matching condition between the two channels. This may be one of the reasons that in the NAL single crystal the mismatch percentage strongly influences the cross-peak intensity, but in the fd bacteriophage sample the effect is much less pronounced (Figure 5(d)). The less specific matching conditions in protein samples further increase the potential spin-exchange pathways, but also may result in the adverse effect that the polarization on the ^{15}N spins can be drained through transferring to the ^{1}H spins.

We have described how the sample motions may partially reverse the inhibition of polarization transfer from "magic-angle" irradiations; however, this still leaves the open question of how the "magic-angle" pulse can produce cross-peak intensities similar to, or even in some case larger than, the on-resonance pulse. One of the reasons may be that "magic-angle" irradiation provides tighter restrictions on polarization transfers than on-resonance irradiation does. Therefore, pathways between a pair of ^{15}N spins may become more local in nature and involve a smaller group of ^{1}H spins. More specifically, magic-angle irradiation strongly suppresses the multiple-step mechanisms and thus reduces the repolarization of ^{1}H spins. Since ^{1}H spins in protein samples usually experience fast decay and short $T_{1\rho}$ relaxation times, the reduction in ^{1}H repolarization may conserve the energy during spin-exchange. The slowdown of decay and conservation of energy is reflected by the polarization reaching maxima at longer contact time when magic-angle irradiation is applied (Figure 5(c)). Another view of spin exchange was recently provided by Khitrin *et al.* based on spin temperature theory,[29] where the authors drew analogy between the on-resonance MMHH pulse sequence and the cross-relaxation driven spin diffusion (CRDSD).[49] The article has only analyzed the on-resonance MMHH pulses, and we have noted the "magic-angle" spin-lock irradiations described here would add additional complication to the situation by slowing down the equilibration in the proton bath. Potentially, the analysis from spin temperature theories on magic-angle irradiation may also contribute important views to the question.

It should also be noted that ^{15}N spins in fd bacteriophage sample are closer in space than those in NAL single crystals, which provides better opportunities for second-order TSAR mechanism to function; however, the ^{1}H-^{15}N dipolar coupling between non-bonded ^{1}H and ^{15}N spins is still very small. We have calculated the orientation-dependent ^{1}H-^{15}N dipolar couplings between the amide groups of residues V29 and V30 based on the structure of the coat protein in intact fd bacteriophage particles.[42] While the directly bonded ^{1}H and ^{15}N have dipolar couplings >6 kHz, the inter-residual dipolar couplings relevant to the TSAR mechanism are only 208 Hz and 167 Hz. Other possible ^{1}H simultaneously coupled to both ^{15}N has dipolar couplings of 410 Hz and 24 Hz, or 167 Hz and 56 Hz. The lack of ^{1}H that can strongly couple to both ^{15}N undermines the efficient spin-exchange through the TSAR mechanism. Nevertheless, we note that a dipeptide single crystal N-acetyl-L-^{15}N-valyl-L-^{15}N-leucine (NAVL) was previously used to monitor spin-exchange for the intramolecular cross-peak between valine and leucine,[27,29] and the comparison of this rigid crystal sample with biological protein sample undergoing rotational motions may be useful for further understanding spin-exchange. The increase of spin-exchange through the TSAR mechanism is likely to work synergistically with the reduction in ^{1}H repolarization and the motion-induced ^{1}H coupling pathways to make magic-angle pulse an efficient condition.

In terms of the practical applications, the angle of the ^{1}H spin-lock irradiation, which can be varied from on-resonance to the "magic-angle," offers a potential way to adjust the range of spin-exchange and provides another degree of freedom to optimize dilute-spin-exchange experiments. Notably, it has also been shown that varying the mismatch percentage can also be used to adjust the range of spin-exchange through the dipolar truncation effect in MMHH experiments.[30] Due to the complexity of spin-exchange mechanisms, optimal conditions may need to be identified empirically for each sample, especially proteins undergoing global reorientation.

C. The comparison of PDSD and MMHH

For ^{15}N-^{15}N spin-exchange in OS solid-state NMR, the comparisons of proton-driven spin diffusion (PDSD) and the recently developed pulse sequences, MMHH or CRDSD, have been made in single crystals[27,29] and membrane proteins in aligned bicelles.[30,50] Depending on the orientation of the single crystal, PDSD was reported to give much higher cross-peak intensity or nearly no cross-peak intensity with up to 4 s mixing. Similarly, with membrane-bound Pf1 coat protein it was shown that the PDSD spectrum had high-intensity cross-peaks for many sequential connections, but also missed several connections that were otherwise shown in MMHH spectra.[30] In our recent application to a mercury transporter protein,[50] similar trends showed that the PDSD spectrum provided a strong cross-peak for one pair of neighboring leucines while it was completely missing for the other pair. The MMHH spectrum showed cross-peaks for both pairs

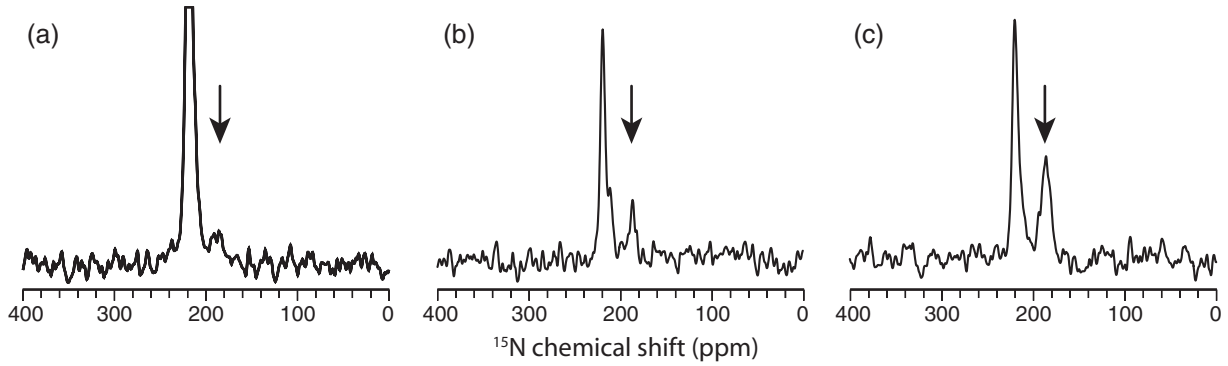

FIG. 6. One-dimensional slices of ^{15}N-^{15}N spin-exchange spectra in the sample of ^{15}N-Val labeled intact fd bacteriophage. Arrows denote the V30-V29 cross-peak. (a) Control spectrum with 0.1 s Z-filter and no MMHH pulse. (b) Magic-angle MMHH spin-exchange spectrum with 7 ms contact time and 22% mismatched amplitude. (c) A 4 s PDSD spin-exchange spectrum. All the spectra are acquired with approximately the same amount of time for reliable comparison of signal to noise, and the plots are scaled to match the same noise level.

of residues, albeit with intensities that were much lower than the single cross-peak observed in the PDSD spectrum.

In the fd bacteriophage sample we systematically optimized the spin exchange conditions. For PDSD experiments, we varied the mixing time between 3 and 6 s. A 4 s mixing time was found to give the largest V29-V30 cross-peak intensity, agreeing with the results obtained from a NAVL single crystal.[27] One of the cross-peaks is compared to the MMHH spectrum and the control experiment in Figure 6. The cross-peak in the PDSD spectrum shows significantly higher intensity than that in the MMHH spectrum, agreeing with previous reports. Notably, we have already taken into account that the amount of time needed to collect each scan is different between MMHH and PDSD experiments, for the fd bacteriophage sample, even with far fewer scans, the cross-peak intensity of the PDSD spectrum is still higher than that of the MMHH spectrum. By contrast, we have found that in the NAL single crystal sample the performance of MMHH mixing exceeds that of PDSD, after taking into account the different amount of time for each experiment. Qualitatively, the higher intensity in the PDSD spectrum compared to the MMHH spectrum is likely due to the differences in T_1 and $T_{1\rho}$ relaxation times. For intact bacteriophage or membrane proteins in aligned bicelles, $T_{1\rho}$ is even shorter than that in a single crystal, leading to a rapid decay of the MMHH cross-peaks.

VI. CONCLUSION

Awareness of the proton-relay mechanism for spin-exchange is important for designing polarization transfer experiments. Switching of the ^{1}H irradiation frequency between on-resonance and off-resonance up to the "magic angle" offers another degree of freedom to optimize the exchange of magnetization, especially for biological samples where substantial motions may be present.

ACKNOWLEDGMENTS

We thank Dr. Alexander A. Nevzorov for discussions that stimulated this research. We thank Dr. Sang Ho Park for discussions about choosing the biological sample, and Dr. Christopher V. Grant and Dr. Chin H. Wu for assistance with instrumentation. The research was supported by Grant Nos. R01GM066978, R01EB005161, and R01GM099986 from the National Institutes of Health. It utilized the Biomedical Technology Resource for NMR Molecular Imaging of Proteins at the University of California, San Diego supported by P41EB002031.

[1]P. Caravatti, G. Bodenhausen, and R. R. Ernst, Chem. Phys. Lett. **89**, 363 (1982).
[2]M. H. Frey and S. J. Opella, J. Am. Chem. Soc. **106**, 4942 (1984).
[3]N. M. Szeverenyi, M. J. Sullivan, and G. E. Maciel, J. Magn. Reson. **47**, 462 (1982).
[4]T. A. Cross, M. H. Frey, and S. J. Opella, J. Am. Chem. Soc. **105**, 7471 (1983).
[5]G. E. Pake, J. Chem. Phys. **16**, 327 (1948).
[6]S. Macura and R. R. Ernst, Mol. Phys. **41**, 95 (1980).
[7]J. Virlet and D. Ghesquieres, Chem. Phys. Lett. **73**, 323 (1980).
[8]J. R. Lewandowski, G. De Paëpe, and R. G. Griffin, J. Am. Chem. Soc. **129**, 728 (2007).
[9]G. De Paepe, J. R. Lewandowski, A. Loquet, A. Bockmann, and R. G. Griffin, J. Chem. Phys. **129**, 245101 (2008).
[10]J. R. Lewandowski, G. De Paëpe, M. T. Eddy, and R. G. Griffin, J. Am. Chem. Soc. **131**, 5769 (2009).
[11]M. Giffard, S. Hediger, J. R. Lewandowski, M. Bardet, J.-P. Simorre, R. G. Griffin, and G. De Paepe, Phys. Chem. Chem. Phys. **14**, 7246 (2012).
[12]A. Nielsen, K. Székely, J. Gath, M. Ernst, N. Nielsen, and B. Meier, J. Biomol. NMR **52**, 283 (2012).
[13]J. M. Lamley, and J. R. Lewandowski, J. Magn. Reson. **218**, 30 (2012).
[14]V. Agarwal, M. Sardo, I. Scholz, A. Böckmann, M. Ernst, and B. Meier, J. Biomol. NMR **56**, 365 (2013).
[15]G. De Paepe, J. R. Lewandowski, A. Loquet, M. Eddy, S. Megy, A. Bockmann, and R. G. Griffin, J. Chem. Phys. **134**, 095101 (2011).
[16]G. De Paëpe, Annu. Rev. Phys. Chem. **63**, 661 (2012).
[17]N. Nielsen, L. Strassø, and A. Nielsen, in *Solid State NMR*, edited by J. C. C. Chan (Springer, Berlin, 2012), p. 1.
[18]B. B. Das, H. J. Nothnagel, G. J. Lu, W. S. Son, Y. Tian, F. M. Marassi, and S. J. Opella, J. Am. Chem. Soc. **134**, 2047 (2012).
[19]I. Bertini, L. Gonnelli, C. Luchinat, J. Mao, and A. Nesi, J. Am. Chem. Soc. **133**, 16013 (2011).
[20]I. Bertini, A. Bhaumik, G. De Paëpe, R. G. Griffin, M. Lelli, J. R. Lewandowski, and C. Luchinat, J. Am. Chem. Soc. **132**, 1032 (2010).
[21]S. Jehle, P. Rajagopal, B. Bardiaux, S. Markovic, R. Kuhne, J. R. Stout, V. A. Higman, R. E. Klevit, B.-J. van Rossum, and H. Oschkinat, Nat. Struct. Mol. Biol. **17**, 1037 (2010).
[22]H. Van Melckebeke, C. Wasmer, A. Lange, E. Ab, A. Loquet, A. Böckmann, and B. H. Meier, J. Am. Chem. Soc. **132**, 13765 (2010).
[23]A. Loquet, N. G. Sgourakis, R. Gupta, K. Giller, D. Riedel, C. Goosmann, C. Griesinger, M. Kolbe, D. Baker, S. Becker, and A. Lange, Nature (London) **486**, 276 (2012).

[24]J.-X. Lu, W. Qiang, W.-M. Yau, C. D. Schwieters, S. C. Meredith, and R. Tycko, Cell **154**, 1257 (2013).
[25]A. A. Nevzorov, J. Am. Chem. Soc. **130**, 11282 (2008).
[26]A. A. Nevzorov, J. Magn. Reson. **201**, 111 (2009).
[27]N. J. Traaseth, T. Gopinath, and G. Veglia, J. Phys. Chem. B **114**, 13872 (2010).
[28]E. C. Lin, and S. J. Opella, J. Magn. Reson. **211**, 37 (2011).
[29]A. K. Khitrin, J. Xu, and A. Ramamoorthy, J. Magn. Reson. **212**, 95 (2011).
[30]W. Tang, R. Knox, and A. Nevzorov, J. Biomol. NMR **54**, 307 (2012).
[31]R. W. Knox, G. J. Lu, S. J. Opella, and A. A. Nevzorov, J. Am. Chem. Soc. **132**, 8255 (2010).
[32]I. Scholz, M. Huber, T. Manolikas, B. H. Meier, and M. Ernst, Chem. Phys. Lett. **460**, 278 (2008).
[33]M. Weingarth, D. E. Demco, G. Bodenhausen, and P. Tekely, Chem. Phys. Lett. **469**, 342 (2009).
[34]A. Lange, K. Seidel, L. Verdier, S. Luca, and M. Baldus, J. Am. Chem. Soc. **125**, 12640 (2003).
[35]A. Grommek, B. H. Meier, and M. Ernst, Chem. Phys. Lett. **427**, 404 (2006).
[36]J.-N. Dumez, M. E. Halse, M. C. Butler, and L. Emsley, Phys. Chem. Chem. Phys. **14**, 86 (2012).
[37]W. I. Goldburg and M. Lee, Phys. Rev. Lett. **11**, 255 (1963).
[38]M. Mehring and V. A. Weberruss, *Object-Oriented Magnetic Resonance: Classes and Objects, Calculations and Computations* (Academic Press, New York, 2001).
[39]I. Bialynicki-Birula, B. Mielnik, and J. Plebański, Ann. Phys. **51**, 187 (1969).
[40]A. Jerschow, J. Magn. Reson. **176**, 7 (2005).
[41]M. H. Levitt, SpinDynamica, 2013, see http://www.SpinDynamica.soton.ac.uk.
[42]A. C. Zeri, M. F. Mesleh, A. A. Nevzorov, and S. J. Opella, Proc. Natl. Acad. Sci. U.S.A. **100**, 6458 (2003).
[43]G. J. Lu, S. H. Park, and S. J. Opella, J. Magn. Reson. **220**, 54 (2012).
[44]G. J. Lu and S. J. Opella, J. Chem. Phys. **139**, 084203 (2013).
[45]A. A. Nevzorov, J. Magn. Reson. **209**, 161 (2011).
[46]W. Tang and A. A. Nevzorov, J. Magn. Reson. **212**, 245 (2011).
[47]G. J. Lu, Y. Tian, N. Vora, F. M. Marassi, and S. J. Opella, J. Am. Chem. Soc. **135**, 9299 (2013).
[48]A. Nevzorov, J. Phys. Chem. B **115**, 15406 (2011).
[49]J. Xu, J. Struppe, and A. Ramamoorthy, J. Chem. Phys. **128**, 052308 (2008).
[50]G. J. Lu and S. J. Opella, J. Biomol. NMR **58**, 69 (2014).
[51]C. H. Wu, C. V. Grant, G. A. Cook, S. H. Park, and S. J. Opella, J. Magn. Reson. **200**, 74 (2009).
[52]F. Delaglio, S. Grzesiek, G. W. Vuister, G. Zhu, J. Pfeifer, and A. Bax, J. Biomol. NMR **6**, 277 (1995).
[53]T. D. Goddard and D. G. Kneller, SPARKY 3, University of California, San Francisco, 2008.
[54]M. Bak, J. T. Rasmussen, and N. C. Nielsen, J. Magn. Reson. **147**, 296 (2000).